This full text paper was peer-reviewed at the direction of IEEE Instrumentation and Measurement Society prior to the acceptance and publication.

Collaborative Localization Sensor for Mobile Robots in Feature-Free Environments

Shengsong Yang, Pierre Payeur
School of Electrical Engineering and Computer Science
University of Ottawa
Ottawa, ON, Canada
[syang123, ppayeur]@uottawa.ca

***Abstract*—Localization for mobile robots has been vastly researched in recent years. However, most solutions remain dependant on the working environment by either extracting information from or installing additional sensors into the environment. An innovative localization sensor is proposed in this work, aiming at providing pose estimation for ground mobile robots while reducing the dependency of the pose estimation on the working environment. The localization approach works under a collaborative scheme where multiple instances of the sensor take relative distance and angular measurements towards each other in order to estimate their respective pose. A mathematical model is derived for the collaborative pose estimation process and two instances of the proposed sensor are implemented and tested with a stationary and a moving landmark to validate the approach.**

Keywords—Localization sensor, ground mobile robots, collaborative pose estimation

I. INTRODUCTION

Mobile robots have become prevalent over the years and localization is one of the most important requirements of their operation. Many localization solutions have been proposed in the literature. Predominant solutions, such as simultaneous localization and mapping (SLAM), tend to rely heavily on already existing features in the working environment or assume consistent environmental conditions. Commercially available solutions, such as Vicon [1] and HTC Vive [2], offer high performance, but sensors must be installed and carefully calibrated in the robots workspace, which is not always possible in time critical applications, and localization can only be performed within the area covered by the fixed sensors.

In this work, an innovative localization sensor and a related pose estimation strategy are proposed and experimentally validated for mobile robotic applications, especially for robotic swarms. Rather than being set in the environment, the sensor is mounted on each ground mobile robot and provides pose estimation with respect to other mobile agents. As such, multiple instances of the sensor work collaboratively to reduce dependency on the working environment while enhancing localization accuracy.

II. RELATED WORK

Taylor-Series estimation [3] is commonly used for localization when geometric information such as distance and bearing measurements between a target to be located and known reference points is given. The solution linearizes an observation model of the measurements and estimates the position of the target iteratively. However, the iterative nature of the solution is unsuitable for online position estimation and convergence of the estimates is not guaranteed. Besides, the reference points are required to be at known positions. Wang and Ho [4] improved the solution by taking into consideration uncertainties residing in the reference locations, but iterations remain heavy.

Fingerprinting [5, 6] has gain popularity in recent years for mobile robotics. This technique harnesses ubiquitous Wi-Fi networks and utilizes the received signal strength (RSS) by devices such as mobile phones. An offline survey is first carried out to record the RSS measurements at chosen reference points over an indoor space. Then, the position of a user device is obtained by comparing its RSS measurements to the stored data. However, multiple Wi-Fi access points should be preinstalled in the environment, and whenever the structure of the environment changes, makeup procedures, such as a new survey, must be carried out.

In recent years, vision and LiDAR-based odometry [7, 8] and simultaneous localization and mapping (SLAM) [9, 10] became popular research topics. Most solutions are feature-based solutions, which utilize features existing in the environment to build a map and provide pose estimation according to a computed map. Alternative solutions, engaging direct methods, estimate positions by minimizing a photometric error in the consecutive images, which is sensitive to drastic environmental changes. Such solutions respond well to man-made and natural outdoor environments that carry rich color or shape texture but degrade in empty, visually uniform or textureless conditions. Given the configuration and data processing constraints imposed by such approaches, localization solutions with limited requirements on the environment still represent an important area of development to support advanced mobile robotics.

III. LOCALIZATION SENSOR CONCEPTUAL DESIGN

Pose estimation with the sensor proposed in this work involves collaborative operation among a number of instances of the device. Each sensor unit carries vision, lidar, and angular measurement instruments, as well as a landmark with a unique color pattern, serving as a unique observable feature. Based on such features, every sensor unit actively monitors all others, forming a collaborative localization sensor network. As a result, pose estimation can be robustly performed without any form of dependency on color or shape textures existing in the

978-1-7281-4460-3/20/$31.00 ©2020 IEEE

environment, contrary to several methods currently used in practice [9, 10]. Actual pose estimation is achieved by measuring the relative distance and angle directly from one sensor unit to other units perceived as visible landmarks, which can be static or moving in the workspace when mounted on a ground mobile robot. A sample scenario with five instances of the proposed sensor is illustrated in Fig. 1. The subscript, $< i, j >$, implies that the corresponding measurement is taken by the i^{th} sensor towards the j^{th} sensor.

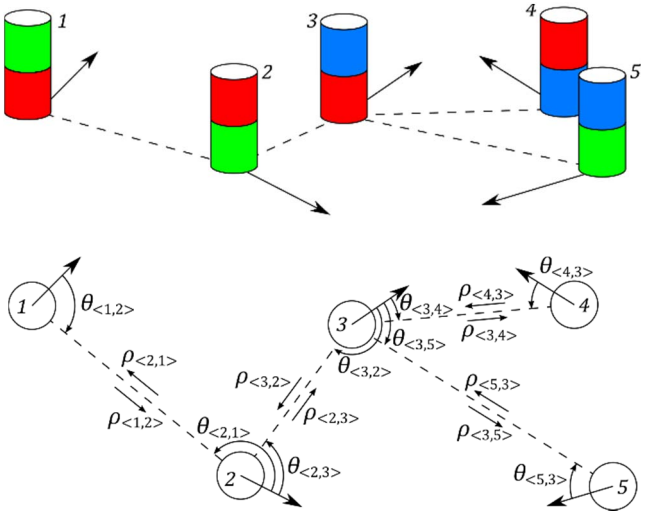

Fig. 1. Example of collaborative localization among five instances of the sensor. Arrows represent respective orientations of the sensor units, and dashed line segments represent relative distances measured by sensor units located at corresponding endpoints.

IV. Localization Sensor Unit Implementation

Beyond the conceptual design, prototypes of the proposed location sensor have been implemented, combining off-the-shelf components in an innovative assembly. Original software solutions were developed and embedded on every sensing unit to support sensors' operation and form a reliable collaborative pose estimation solution.

A. Physical Sensor Unit Assembly

On each sensor unit, a laser rangefinder is employed to measure distances, the orientation of which is rotated horizontally by a full-revolution servo motor. A relative distance measurement is collected when the rangefinder is pointed towards another sensor unit, which carries its own landmark. The relative angular measurement is simultaneously collected by an absolute encoder encapsulated in the servo motor. To permit automated and collaborative operation among the sensor units, a color camera is also integrated on every unit to visually detect and track embedded landmarks. The orientation of the camera is mechanically aligned with that of the rangefinder so that a detected landmark is centered on the image when the rangefinder takes measurements.

One objective of this work is to develop a versatile sensor device that can readily be installed over a wide variety of ground mobile robots with no need for mechanical, electronic or software modifications of the robotic platform. Therefore, the localization sensor should be sufficiently compact and not interfere with the original routines of the robots. In addition, the localization sensor should be installed with a known relative pose with respect to the host robot so that the pose of each robot can be estimated by applying transformations on the estimated pose of the localization sensor that a robot carries. The prototype sensor unit, shown in Fig. 2, has a dimension of 200×200×350 mm and is mounted on a compact Turtlebot3 Waffle Pi robot for demonstration. To provide reliable relative measurements among the sensor units, the rotation center of the rangefinder is considered as the center of the sensor unit and the landmark is installed right on top of the center.

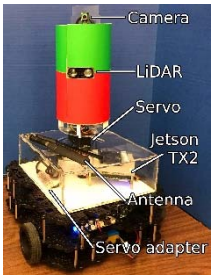

Fig. 2. Prototype localization sensor mounted on a Turtlebot3 Waffle Pi robot.

To validate the concept, two instances of the proposed localization sensor were implemented. Every unit integrates a See3CAM USB camera, a Garmin LiDAR Lite v3, and a Dynamixel XL430-W250T servo motor. The color-coded landmark is made from a Uline kraft mailing tube with a radius of 53 mm and a height of 200 mm. One unit employs a Jetson TX2 module as its embedded processor, while the other uses a Jetson Nano kit instead. Both units can communicate wirelessly and send their measurements to a laptop computer, where the collaborative pose estimation of the sensor units takes place.

B. Landmark Detection and Tracking

As shown in Fig. 2, the cylindrical landmark which forms the upper section of the localization sensor consists of a combination of two vertically neighboring sections with distinct colors. Every landmark is formed by a different color pair to assign a unique identifier to every unit. To detect and track the landmark, a sampling-based algorithm is developed by improving the work presented in [11].

The position of the landmark center on the color image is considered as a random variable and represented by many weighted samples. Due to lacking knowledge of the relative motion of the sensor units, the velocity of the landmark center on the image is also considered as a random variable. Large variance is added to both random variables to counteract the varying relative locations among the units. In case that the algorithm loses track of the landmark, the variance drives the samples to diverge from each other to search over a larger area, which provides support for landmark recovery.

At each time step, the position of each sample is first predicted and the weight of each sample is updated. Then a resampling process is carried out so that the samples will propagate towards those with higher weights. An improved weight-updating model is proposed and illustrated in Fig. 3, where the black dot represents the position of a sample and the white circles represent pixels of which the colors are compared to the known colors on the landmark to be detected. The number of pixels for each sample is selected empirically to trade off

computational speed for increased robustness to environmental noise. A large constant weight is assigned to a sample if the HSV components of all the colors at the chosen pixels are within a pre-set range from that of the color-coded landmark, otherwise, a small constant weight is assigned. Therefore, the samples will eventually center on the color transition part of the landmark instead of forming a unimodal distribution, as in [11], which is prone to noise.

The distance between the upper and lower pixels is also considered as a positive random variable updated at each time step to adapt for the varying size of the landmark on the image, whose scale changes with distance. The framework of the improved algorithm is developed based on the MRPT library [12]. An illustration of the landmark detection process is shown in Fig. 4, where samples are shown at their positions as cyan dots. Scenes are displayed for cases where color-coded landmarks are respectively occluded or fully visible. These results demonstrate the capability of the landmark detection approach to search over a wide surface for a recognizable landmark, while being robust to a complex textured background.

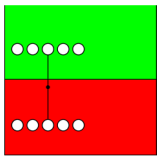

Fig. 3. Proposed model for updating each sample's weight.

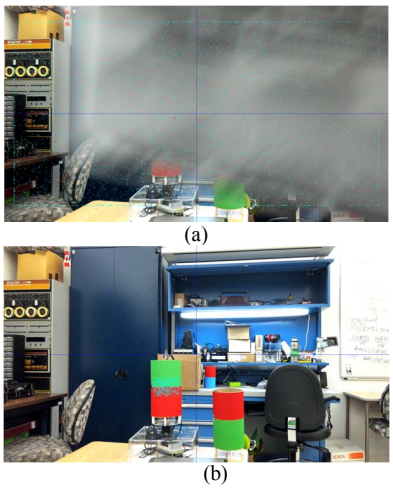

Fig. 4. Visual landmark detection process: (a) samples spread all over the image when the landmark is not detected; (b) the landmark (green top & red bottom) is detected by samples after it is revealed.

A small variance on the position of the samples indicates a successful detection. The position of the landmark center is acquired as the average position of all samples. Based on the relative direction over the horizon where the landmark is detected, the localization sensor unit rotates to automatically adjust the orientation of the camera and the rangefinder before initiating measurements. If the variance is larger than an empirically set threshold, meaning no landmark has been detected, the sensor unit will rotate around and search for a landmark with predefined colors. This process provides the sensor unit with the capability to automatically search for and keep track of other units and therefore estimate the motion of a corresponding mobile robot on which a sensor unit is also installed.

C. Sensor Characterization

Both prototype sensor units were experimentally characterized to analyze their behavior and accuracy. Noise in the distance and angular measurements from the two units is modeled as Gaussian white noise, but with different variance.

The standard deviation of distance measurements is characterized by collecting samples on a flat panel placed at various distances, with knowledge of ground truth values. At each distance, 1000 measurements are collected and statistically analyzed. For angular measurements, it is assumed that the absolute encoders encapsulated in the servo motors provide accurate feedback on motor states, and the error in the angular measurements is considered to be mainly related to the landmark detection and tracking algorithm, described in Section IV.B, which is strongly correlated to the distance between the landmark and the localization sensor. Angular measurements are collected over a landmark placed in front of the two sensor units at known distances and 200 measurements are collected at each distance. The standard deviations observed on distance and angular measurements from the two prototype units are depicted in Fig. 5 and Fig. 6, respectively.

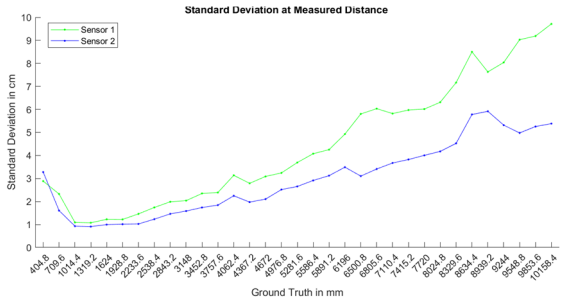

Fig. 5. Standard deviation on distance measurements from two sensor units.

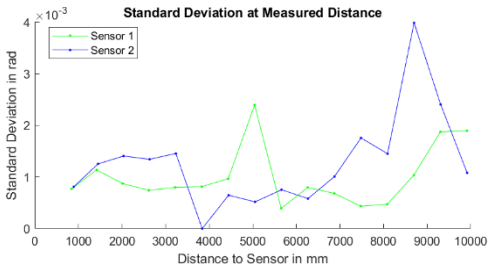

Fig. 6. Standard deviation on angular measurements from two sensor units.

The standard deviation on distance measurements shows a tendency to increase with the ground truth distance. It is noticeable that Sensor 2 has slightly better performance than Sensor 1. On the other hand, the standard deviation of angular measurements does not present an obvious correlation to the distance between the landmark and the two sensor units.

On the prototype sensor units, the standard deviation on the measurements is interpolated among the acquired values at each pre-set distance, shown as dots in Fig. 5 and Fig. 6. Considering a Gaussian error model, the posterior probability density functions of the ground truth values, d and θ, given N measurements, $\{d_{mi}\}$ and $\{\theta_{mi}\}$, can be derived as:

$$p(d\,|\{d_{mi}\}) = \frac{1}{\sqrt{2\pi\sigma_d^2}}\exp\left(-\frac{(d-\mu_d)^2}{2\sigma_d^2}\right) \quad (1)$$

$$p(\theta|\{\theta_{mi}\}) = \frac{1}{\sqrt{2\pi\sigma_\theta^2}}\exp\left(-\frac{(\theta-\mu_\theta)^2}{2\sigma_\theta^2}\right) \quad (2)$$

where $\mu_d = \frac{1}{N}\sum_{i=1}^{N} d_{mi}$, $\sigma_d^2 = \frac{1}{N}\sigma_{d_m}^2$, $\mu_\theta = \frac{1}{N}\sum_{i=1}^{N}\theta_{mi}$, and $\sigma_\theta^2 = \frac{1}{N}\sigma_{\theta_m}^2$. The standard deviations, σ_{d_m} and σ_{θ_m}, are interpolated at μ_d and μ_θ, respectively according to Fig. 5 and Fig. 6.

V. Derivation of Localization Methods

The pose estimation for the proposed localization sensor is divided into two procedures: position estimation and inter-calibration. First, the position of a sensor unit can be solely estimated based on measurements made by other sensor units. Second, measurements of the unit itself on the other ones are also taken into consideration for the sensor to inter-calibrate with other units. As such, the orientation of the sensor unit can then be determined, and the position initially estimated by other units is refined.

A. Individual and Collaborative Position Estimation

Since raw measurements are made against the colored landmark that is part of every localization sensor, the position of the unit being estimated is considered the same as that of the landmark.

Given that distance measurements are collected on the outside of the cylindrical landmarks, the radius of the landmark is added to the measurements to estimate the actual distance between two sensor units. Given the relative distance and angle, $[\rho, \theta]^T$, between a sensor unit at $\boldsymbol{s} = [u, v]^T$ with orientation ϕ and a landmark at $\boldsymbol{x} = [x, y]^T$, the coordinates of the landmark can be expressed as:

$$\boldsymbol{x} = \begin{bmatrix} x \\ y \end{bmatrix} = \begin{bmatrix} \rho\cos(\theta+\phi) + u \\ \rho\sin(\theta+\phi) + v \end{bmatrix} \quad (3)$$

By linearizing the above transformation at the measurement, $\boldsymbol{r}_m = [\rho_m, \theta_m]^T$, the position of the landmark can be approximated as:

$$\boldsymbol{x} \approx \boldsymbol{x}_m + \boldsymbol{J}(\boldsymbol{r}_m)\begin{bmatrix} \rho - \rho_m \\ \theta - \theta_m \end{bmatrix} \quad (4)$$

where $\boldsymbol{J}(\boldsymbol{r}_m) = \begin{bmatrix} cos(\theta_m+\phi) & -\rho_m\, sin(\theta_m+\phi) \\ sin(\theta_m+\phi) & \rho_m\, cos(\theta_m+\phi) \end{bmatrix}$ is the Jacobian matrix of the transform provided in (3), and $\boldsymbol{x}_m = \begin{bmatrix} \rho_m\cos(\theta_m+\phi) + u \\ \rho_m\sin(\theta_m+\phi) + v \end{bmatrix}$. Following the above linearization, the position of the landmark, represented as a 2-D Gaussian distribution, is given by:

$$\boldsymbol{x} \sim N(\boldsymbol{x}_m, \boldsymbol{\Sigma}_{\boldsymbol{x}_m}) \quad (5)$$

where $\boldsymbol{\Sigma}_{\boldsymbol{x}_m} = \boldsymbol{J}(\boldsymbol{r}_m)\boldsymbol{\Sigma}_{\boldsymbol{r}_m}\boldsymbol{J}^{\boldsymbol{T}}(\boldsymbol{r}_m)$ and $\boldsymbol{\Sigma}_{\boldsymbol{r}_m} = diag(\sigma_{\rho_m}^2, \sigma_{\theta_m}^2)$. In case that the position and orientation of the sensor unit are given as Gaussian distributions, where $\boldsymbol{s} \sim N(\boldsymbol{s}_m, \boldsymbol{\Sigma}_{\boldsymbol{s}_m})$ and $\phi \sim N(\phi_m, \sigma_{\phi_m}^2)$, the estimated position of the landmark and its covariance matrix are given as:

$$\boldsymbol{x}_m = \begin{bmatrix} \rho_m\, cos(\phi_m+\theta_m) + u_m \\ \rho_m\, sin(\phi_m+\theta_m) + v_m \end{bmatrix} \quad (6)$$

$$\boldsymbol{\Sigma}_{\boldsymbol{x}_m} = \boldsymbol{J}_g\left(\begin{bmatrix} \rho_m \\ \phi_m+\theta_m \end{bmatrix}\right)\begin{bmatrix} \sigma_\rho^2 & 0 \\ 0 & \sigma_\theta^2+\sigma_\phi^2 \end{bmatrix}\boldsymbol{J}_g^{\boldsymbol{T}}\left(\begin{bmatrix} \rho_m \\ \phi_m+\theta_m \end{bmatrix}\right) + \boldsymbol{\Sigma}_{\boldsymbol{s}_m} \quad (7)$$

where $\boldsymbol{J}_g\left(\begin{bmatrix} \rho_m \\ \phi_m+\theta_m \end{bmatrix}\right) = \begin{bmatrix} \cos(\phi_m+\theta_m) & -\rho_m\sin(\phi_m+\theta_m) \\ \sin(\phi_m+\theta_m) & \rho_m\cos(\phi_m+\theta_m) \end{bmatrix}$.

When estimating the position of the landmark using multiple instances of the localization sensor, assuming R instances, the collaboratively estimated position is the weighted average of all individual position estimates. The estimated position and its covariance matrix are then given as:

$$\boldsymbol{x}_m = \left(\sum_i^R \boldsymbol{\Sigma}_{\boldsymbol{x}_{mi}}^{-1}\right)^{-1}\sum_i^R\left(\boldsymbol{\Sigma}_{\boldsymbol{x}_{mi}}^{-1}\boldsymbol{x}_{mi}\right) \quad (8)$$

$$\boldsymbol{\Sigma}_{\boldsymbol{x}_m} = \left(\sum_i^R \boldsymbol{\Sigma}_{\boldsymbol{x}_{mi}}^{-1}\right)^{-1} \quad (9)$$

where $\boldsymbol{x}_{mi}$ is the individual position estimate by the i^{th} instance of the sensor and $\boldsymbol{\Sigma}_{\boldsymbol{x}_{mi}}$ is its covariance matrix.

B. Collaborative Inter-Calibration

If an instance of the localization sensor inter-calibrates with other instances whose poses are known, the orientation of the instance can then be estimated, and the previously developed position estimation model can be refined.

Assume the position and orientation of Sensor C, denoted by $\boldsymbol{s}_C = [u_C, v_C]^T$ and ϕ_C, are unknown, and Sensor C inter-calibrates with R sensor units, whose position and orientation are given as $\boldsymbol{s}_i \sim N(\boldsymbol{s}_{mi}, \boldsymbol{\Sigma}_{\boldsymbol{s}_{mi}})$ and $\phi_i \sim N(\phi_{mi}, \sigma_{\phi_{mi}}^2)$, respectively, and $i = 1,2,\dots,R$. Denote the measurements made by Sensor i to Sensor C as $\boldsymbol{r}_{m<i,C>} = \left[\rho_{m<i,C>}, \theta_{m<i,C>}\right]^T$, and the measurements made by Sensor C to Sensor i as $\boldsymbol{r}_{m<C,i>} = \left[\rho_{m<C,i>}, \theta_{m<C,i>}\right]^T$. The corresponding true values of the measurements are given by $\boldsymbol{r}_{<i,C>} = \left[\rho_{<i,C>}, \theta_{<i,C>}\right]^T$ and $\boldsymbol{r}_{<C,i>} = \left[\rho_{<C,i>}, \theta_{<C,i>}\right]^T$, and the orientation of Sensor C, ϕ_C, is given by:

$$\phi_C = \pi + \phi_i + \theta_{<i,C>} - \theta_{<C,i>} \quad (10)$$

Thus, ϕ_C has a Gaussian distribution inter-calibrating with the i^{th} sensor unit, $\phi_C \sim N(\phi_{mC\{i,C\}}, \sigma_{mC\{i,C\}}^2)$, where $\sigma_{mC\{i,C\}}^2 = \sigma_{\theta_{m<i,C>}}^2 + \sigma_{\phi_{mi}}^2 + \sigma_{\theta_{m<C,i>}}^2$ and $\phi_{mC\{i,C\}} = \pi + \phi_{mi} + \theta_{m<i,C>} - \theta_{m<C,i>}$. The collaboratively inter-calibrated orientation of Sensor C is then derived as $\phi_{mC} = \sum_i^R \frac{\phi_{mC\{i,C\}}}{\sigma_{\phi_{mC\{i,C\}}}^2} / \sum_i^R \frac{1}{\sigma_{\phi_{mC\{i,C\}}}^2}$, and its variance is given by $\sigma_{\phi_{mC}}^2 = \sum_i^R \frac{1}{\sigma_{\phi_{mC\{i,C\}}}^2}$.

Since both Sensor C and Sensor i are measuring over the same distance in between the two sensor units and the measurements are independent of each other, a more reliable estimated distance can be acquired as the weighted average of the distance measurements from both instances. The inter-calibrated distance and its variance are given by:

$$\rho_{m\{i,C\}} = \frac{\frac{1}{\sigma_{\rho m<i,C>}^2}\rho_{m<i,C>} + \frac{1}{\sigma_{\rho m<C,i>}^2}\rho_{m<C,i>}}{\frac{1}{\sigma_{\rho m<i,C>}^2} + \frac{1}{\sigma_{\rho m<C,i>}^2}} \quad (11)$$

$$\sigma^2_{\rho_{m\{i,C\}}} = \frac{1}{\frac{1}{\sigma^2_{\rho_{m<i,C>}}} + \frac{1}{\sigma^2_{\rho_{m<C,i>}}}} \quad (12)$$

The subscript using curly brackets indicates that the identities inside are interchangeable. The inter-calibrated distance could then be substituted in the previously developed position estimation models to improve the performance of the localization sensor.

VI. Experimental Validation and Results

The performance of two implemented prototypes of the localization sensor is validated through experiments considering respectively stationary and moving landmarks in an indoor environment. The experiments are designed to validate the proposed position estimation provided in Section V.A. The methodology provided in Section V.B has been validated in simulation only as the availability of a third unit of the localization sensor would be required. Throughout the experiments, each sensor unit is fixed at a location, the actual value of which is determined by the Taylor-Series estimation [3]. Before each experiment, distance and angular measurements are collected against a landmark manually placed at several known positions to estimate the respective pose of each sensor unit, and the measurements used for the process are not reused in any of the following experiments.

A. Position Estimation on a Stationary Landmark

The instances of the localization sensor are first tested for estimating the position of a stationary landmark both individually and collaboratively. In the experiment, two sensor units are fixed at one end of the working area, while a testing landmark is manually and successively placed at known positions. A total number of 90 positions are measured over a working area of about 3×10 meters. The individual and collaborative position estimates are shown in Fig. 7. The respective sensor units are shown at the bottom left corner, with Sensor 1 in green and Sensor 2 in blue. At about (7000, 3000), outliers are connected to the corresponding ground truth by straight lines.

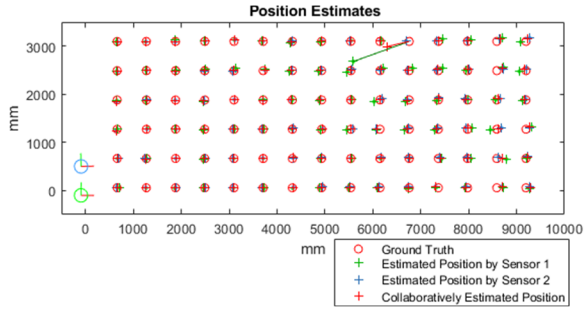

Fig. 7. Individual and collaborative position estimates by two localization sensor units.

The bidimensional position estimation error is defined as the Euclidean distance between an estimated position and its actual value, defined as

$$\epsilon_{position} = \|\boldsymbol{x}_{estimated} - \boldsymbol{x}_{actual}\| \quad (13)$$

The experimental position estimation errors for the individual and collaborative position estimations are shown in Fig. 8 and Fig. 9.

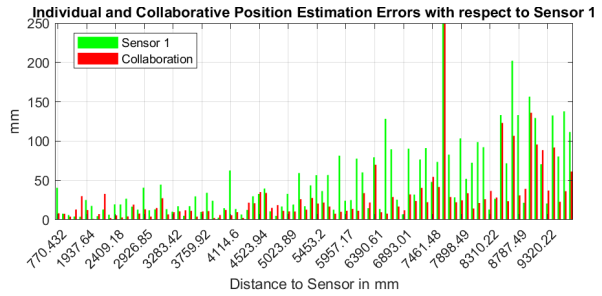

Fig. 8. Individual position estimation errors by Sensor 1 and collaborative position estimation errors by both units.

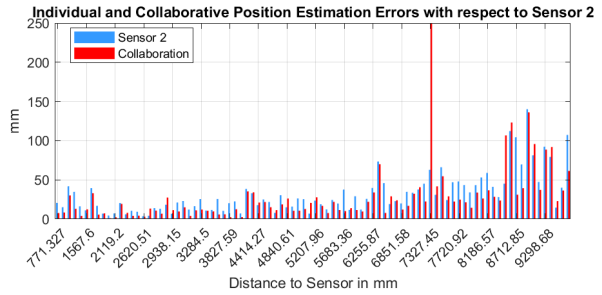

Fig. 9. Individual position estimation errors by Sensor 2 and collaborative position estimation errors by both units.

The two implemented instances of the localization sensor exhibit different performances in individual position estimation. Sensor 1 tends to have larger estimation errors than Sensor 2, which corresponds to their respective characteristics observed in Section IV.C, where Sensor 1 revealed a larger standard deviation on distance measurements. Both sensor units progressively increase their individual position estimation error at distances over 8.3 meters. The increase is a consequence of the cylindrical landmark failing to fully reflect the laser beam emitted by the rangefinder as its dispersion increases over the distance and reaches beyond the width of the landmark cylinder, 53 mm, at about 8.3 m. As a result, background surfaces in the testing environment start to contribute to the distance measurements. Therefore, the sensor units are considered to provide reliable position estimation within 8.3 meters. Within this range, Sensor 2 has reached a maximum estimation error of about 75 mm, but most errors are within 50 mm. At shorter distances, significantly smaller errors are observed, which is coherent with the sensor's characterization curve presented in Fig. 5. Sensor 1 also exhibits smaller errors at closer distances, but error grows more rapidly when distance increases. Overall, a maximum error of about 130 mm is observed by Sensor 1 within the reliable working range of 8.3 m. Such error is larger than that of commercially available solutions mentioned earlier [1, 2], which reportedly have typical errors smaller than 1 mm. However, the proposed localization sensor has a much longer working distance of 8.3 meters and no system setup is required. When compared to visual odometry and SLAM solutions [8, 9, 10], the proposed localization sensor also offers substantial benefits from its independence from the working environment.

Fig. 8 and Fig. 9 show that the proposed collaborative position estimation strategy between the two sensor units systematically reduces the estimation error, depicted as red bars, and successfully compensates for the larger deviations observed

on Sensor 1, resulting in the smallest estimation errors at most measured landmark positions.

B. Position Estimation on a Moving Landmark

The second experiment demonstrates the capability of the prototype sensor units to localize a moving landmark, as involved in tracking a mobile robot. The sensor units are fixed at one end of the working area, while a Turtlebot3 Waffle Pi robot carrying a color-coded landmark follows a zig-zag path at a speed of 0.1 m/s. The mobile robot is equipped with a laser scanner onboard, which acquires 2-D laser scans, and an odometry sensor providing odometry data of the robot. A Monte-Carlo localization method [13], utilizing a 2-D occupancy map built before the experiments using GMapping [14], is compared to the performance achieved with the prototype sensor units. Due to the fact that the ground truth of the landmark position is not accessible in this case since the mobile robot was manually piloted along the trajectory, results are evaluated qualitatively.

The successive locations of the moving landmark are shown in Fig. 10. Position estimates from Sensor 1 and Sensor 2 are shown as green and blue dots, respectively, while those from the Monte-Carlo approach are shown as red dots. The mobile robot follows the zig-zag path from the left to the right on the map.

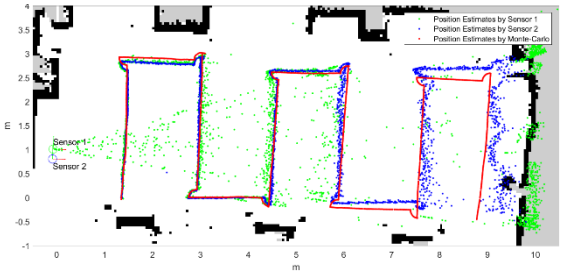

Fig. 10. Position estimates of a moving landmark by two prototype sensor units and the Monte-Carlo localization method.

The two prototype sensor units are successful at tracking the mobile robot. A similar performance of the units is observed to that in the previous experiment but increasing estimation biases can be observed at long distances, with Sensor 1 generating more outliers. The units have very similar position estimates when compared to the Monte-Carlo approach at closer distances. At long distances, the localization sensor units have larger variances because of the rangefinders, as characterized in Section IV.C, and the Monte-Carlo approach is subject to errors from the accumulated odometry data and the accuracy of the map. It is worth noting that the Monte-Carlo approach requires existing features in the environment, while the proposed localization sensor units have little reliance on the environment, which makes the proposed approach readily accessible for a vast range of applications.

The experimental results obtained from two prototypes of the first generation of collaborative localization sensor units demonstrate the feasibility of the original concept that is proposed in this work.

VII. Conclusion

In this paper, an innovative localization sensing strategy that leverages collaborative sensor devices to estimate the pose of ground mobile robots without a dependency on observable features in the working environment is proposed and experimentally validated. The implementation of two prototype instances of the sensing unit along with original collaborative pose estimation frameworks is detailed. Experimental validation with a stationary landmark and a mobile robot demonstrated the sensor's capability to reliably estimate position up to about 8 meters. These encouraging results open the door for applications of the localization approach in real-world scenarios for swarm robotics when individual robots jointly evolve in a workspace. Future work will involve refining the embedded laser rangefinder devices and implementing individual rectification of raw measurements. Moreover, the framework will be expanded to a larger number of sensor units working in collaboration in order to further leverage the gain in accuracy demonstrated in this work, as a result of a collaborative pose estimation strategy.

References

[1] M. Windolf, N. Götzen, and M. Morlock, "Systematic Accuracy and Precision Analysis of Video Motion Capturing Systems-Exemplified on the Vicon-460 System," *J. Biomech.*, vol. 41, no. 12, pp. 2776–2780, 2008.

[2] M. Borges, A. Symington, B. Coltin, T. Smith, and R. Ventura, "HTC Vive: Analysis and Accuracy Improvement," *IEEE Int. Conf. Intell. Robot. Syst.*, pp. 2610–2615, 2018.

[3] W. Foy, "Position-Location Solutions by Taylor-Series Estimation," *IEEE Trans. Aerosp. Electron. Syst.*, vol. AES-12, no. 2, pp. 187–194, Mar. 1976.

[4] Y. Wang and K. C. Ho, "An Asymptotically Efficient Estimator in Closed-Form for 3-D AOA Localization Using a Sensor Network," *IEEE Trans. Wirel. Commun.*, vol. 14, no. 12, pp. 6524–6535, 2015.

[5] S. He and S. H. G. Chan, "Wi-Fi Fingerprint-based Indoor Positioning: Recent Advances and Comparisons," *IEEE Communications Surveys and Tutorials*, vol. 18, no. 1. pp. 466–490, 2016.

[6] S. He, S. H. G. Chan, L. Yu, and N. Liu, "SLAC: Calibration-Free Pedometer-Fingerprint Fusion for Indoor Localization," *IEEE Trans. Mob. Comput.*, vol. 17, no. 5, pp. 1176–1189, 2018.

[7] K. Lingemann, H. Surmann, A. Nüchter, and J. Hertzberg, "Indoor and Outdoor Localization for Fast Mobile Robots," in *IEEE/RSJ International Conference on Intelligent Robots and Systems (IROS)*, 2004, vol. 3, pp. 2185–2190.

[8] J. Engel, V. Koltun, and D. Cremers, "Direct Sparse Odometry," *IEEE Trans. Pattern Anal. Mach. Intell.*, vol. 40, no. 3, pp. 611–625, Jul. 2016.

[9] J. Engel, T. Schöps, and D. Cremers, "LSD-SLAM: Large-Scale Direct Monocular SLAM," *Lect. Notes Comput. Sci.* (including Subser. Lect. Notes Artif. Intell. Lect. Notes Bioinformatics), pp. 834–849, 2014.

[10] R. Mur-Artal and J. D. Tardos, "ORB-SLAM2: An Open-Source SLAM System for Monocular, Stereo, and RGB-D Cameras," *IEEE Trans. Robot.*, vol. 33, no. 5, pp. 1255–1262, 2017.

[11] G. Jang, S. Kim, W. Lee, and I. Kweon, "Color Landmark Based Self-Localization for Indoor Mobile Robots," in *Proceedings - IEEE International Conference on Robotics and Automation*, 2002, pp. 1037–1042.

[12] J. Claraco, "Contributions to Localization, Mapping and Navigation in Mobile Robotics," *Univ. Málaga, Málaga*, 2009.

[13] D. Fox, W. Burgard, F. Dellaert, and S. Thrun, "Monte Carlo Localization: Efficient Position Estimation for Mobile Robots," *Proc. Natl. Conf. Artif. Intell.*, pp. 343–349, 1999.

[14] G. Grisetti, C. Stachniss, and W. Burgard, "Improved Techniques for Grid Mapping with Rao-Blackwellized Particle Filters," *IEEE Trans. Robot.*, vol. 23, no. 1, pp. 34–46, 2007.